Self-calibrated, line-scan STED-FCS to quantify lipid dynamics in model and cell membranes

Aleš Benda, Yuanqing Ma and Katharina Gaus

Centre for Vascular Research, Australian Centre for Nanomedicine and ARC Centre of Excellence in Advanced Molecular Imaging, University of New South Wales, Sydney NSW
[#] **Correspondence to**: k.gaus@unsw.edu.au

THEORY

Resonant line-scan spatio-temporal correlation function calculation

Line-scan FCS is based on the spatio-temporal correlation of fluorescence intensities obtained by fast scanning of a detection volume along a fixed line within a sample (1). The time evolution of spatially dependent fluorescence intensity can be visualized by an *xt* image, also called kymograph or intensity carpet (Fig 1c,d). By correlating the kymograph data in both dimensions, a spatio-temporal correlation *G(kΔx,lΔt)* is obtained:

$$G(k\Delta x, l\Delta t) = \left(\sum_{i=0}^{n_x-1} \sum_{j=0}^{n_t-1} I(i,j) I(i+k, j+l) \right) \frac{n_x}{n_x - |k|} \frac{n_t}{n_t - |l|} \qquad (1)$$

where *Δx* is a pixel size, *Δt* is the time difference between two consecutive lines (line time), *k* and *l* are integer indexes of distance and time, *I(i,j)* is the intensity value of pixel *i* and *j* in the kymograph, n_x is the total number of pixels and n_t is the total number of lines.

The correlation function can be calculated by direct multiplication (1) or by fast Fourier transform (2). These straightforward approaches can be directly applied to intensity *xt* images obtained by standard acquisition software and are not limited to single photon counting detection. The pixel size should be much smaller than the radius of the detection spot and the maximal spatial distance for which the correlation is calculated should cover distances that the molecules can diffuse across within the acquisition time. The spacing of time correlation points must range from single line time to overall acquisition time. Typically this is best achieved by using a multiple-tau correlation scheme. However, the direct calculation of spatio-temporal correlation covering the required spatial and time resolution is extremely time consuming. Hence we introduced a new faster algorithm based on single photon data format.

The fluorescence intensity is detected as single photon events and stored in a time-tagged time resolved data format with inbuilt markers for synchronization with the scanner (TTTR, PicoQuant, Germany). In the case of a resonant scanner, the position *a* of the focus is a sine function of time *t*:

$$a = A\sin(2\pi f t + \varphi) \qquad (2)$$

Where *A* is the amplitude, *f* is the resonant frequency of the scanner and ϕ is the phase shift. The amplitude *A* depends on the zoom and the objective used. The typical settings of the zoom at 30-times in conjunction with a 1.4NA 100x oil immersion objective give an amplitude of 3217 nm. The resonant frequency of the used scanner was 7920 Hz. The basic unit of lag-time is equal to the line period, which is 63 µs for a bidirectional scan at 7920 Hz.

In accordance with the multiple-tau correlation scheme, the temporal sampling consists of several levels of linear ranges, each range having double the sampling of the previous level. The spatial sampling is given by the frequency of the pulsed excitation laser or the photon detection unit for cw excitation. The finite time sampling means that the photon detection positions are finite as well, giving a definite number of realizations for each distance difference.

The spatio-temporal correlation function is calculated from raw TTTR data in the following steps:

1. The start times of each forward and backward line are obtained from the synchronization markers. This involves interpolation of markers' time to compensate for the 1 MHz markers under-sampling and a phase shift correction. The phase shift as determined from calibration is typically -0.8434. Phase shift calibration is based on maximizing temporal correlation function at zero distance between forward and backward lines for lag times up to 16 lines.
2. Knowing the line start times, each photon is assigned a line (time) number and a precise position along the scanned line.
3. A histogram $H(\delta,\tau)$ of time τ and position δ differences is obtained by comparing line numbers and positions of all photons.

$$H(\delta,\tau) = \sum_{i=0}^{n}\sum_{j=0}^{n,j\neq i}\begin{cases} w_i w_j \text{ if } \left(\delta-\frac{\Delta}{2}\right) < (a_i - a_j) < \left(\delta+\frac{\Delta}{2}\right) \text{ and } \left(\tau-\frac{T}{2}\right) < (t_i - t_j) < \left(\tau+\frac{T}{2}\right) \\ 0 \quad \text{elsewhere} \end{cases} \quad (3)$$

where n is the total number of photons, w_i is the photon weight (intensity), a_i is the position and t_i is the time of i-th detection event, Δ is the spatial correlation sampling and T is the temporal sampling for the given correlation level.

The histogram is calculated for linear spacing of distances and semi-logarithmic spacing in time (multiple-tau algorithm). The algorithm accepts real values of photon intensity, which makes it suitable for photon weighting required for filtered FCS.

4. The correlation function is obtained by correcting the values in a histogram with the relative number of possible occurrences of the given distance-time pair compared to zero distance zero time difference pair. The spatial correction $C_S(\delta)$ is derived from a possible number of realizations of the given distance δ and corrects for both nonlinear scanner motion and average intensity line profile, and is given by: $C_s(\delta) =$

$$\sum_{i=0}^{m}\sum_{j=0}^{m,j\neq i}\begin{cases} I_i I_j \text{ if } \left(\delta-\frac{\Delta}{2}\right) < (a_i - a_j) < \left(\delta+\frac{\Delta}{2}\right) \\ 0 \quad \text{elsewhere} \end{cases} \quad (4)$$

where m is the number of sampling points covering the selected part of the scanned line, I_i is the overall intensity in the given sampling point, a_i is the position of the sampling point and Δ is the spatial correlation sampling.

The time correction $C_T(\tau)$ accounts for varying temporal sampling of correlation function, for finite length of the measurement and is given by:

$$C_T(\tau) = (floor\left(\frac{t}{T}\right) - \tau/T)/T^2 \quad (5)$$

where t is the total measurement time in number of lines and T is the temporal sampling for the given correlation level in number of lines.

The corrected spatio-temporal correlation function $G(\delta,\tau)$ is then given by:

$$G(\delta,\tau) = H(\delta,\tau)\frac{C_S(0)}{C_S(\delta)}\frac{C_T(0)}{C_T(\tau)} \quad (6)$$

5. The optional correction for homogenous photobleaching is based on the fact that the decrease in the average number of dye molecules in the detection spot as measurement progresses only changes the non-correlated offset at different lag times for raw correlation data without intensity normalization. The offset for each lag time is estimated directly from the correlation function, assuming that at long distances there is no correlation at full time scale. The photobleaching corrected spatio-temporal correlation function $G_{PC}(\delta,\tau)$ is then given by:
$$G_{PC}(\delta,\tau) = G(\delta,\tau) + G(\delta_{max},0) - G(\delta_{max},\tau) \quad (7)$$
where δ_{max} is the maximal distance for which the correlation function was calculated.
6. The final step is an optional intensity normalization, in which first a constant offset is subtracted from the correlation function and the result is then divided by the constant offset. As a result the amplitude of correlation function is inversely proportional to the number of dye molecules in the detection spot. The intensity normalized spatio-temporal correlation function $G_{IN}(\delta,\tau)$ is then given by
$$G_{IN}(\delta,\tau) = (G(\delta,\tau) - G(\delta_{max},0))/G(\delta_{max},0) \quad (8)$$

The presented correlation function calculation scheme is not restricted to TTTR or other single photon data acquisition formats, but can also be used for *xt* image based data formats. First the pixel shift is determined by maximizing temporal correlation function at zero distance between odd and even (forward and backward) lines for lag times up to 16. In a second step *xt* images are converted to single photon format. The weight of the photon is an intensity of the pixel. Zero pixel intensity means that no photon event is generated. The number of the pixel is converted to a position and the line number into its time.

Filtered FCS

Filtered FCS (fFCS) is a more general term for mathematically identical fluorescence lifetime correlation spectroscopy (FLCS) (3, 4), originally invented under the name time-resolved fluorescence correlation spectroscopy (5). The difference is that in the case of FLCS the species are resolved based on differences in their excited state lifetime behavior, whereas in the more general case of filtered FCS the species are resolved based on their different patterns in multichannel detection. The different patterns also include different excited state lifetimes, but in addition to that they can also include spectral differences (6), anisotropy differences (7) and spatial excitation modulation differences (8).

Briefly at every time t, the fluorescence intensity $I_j(t)$ in each detection channel j is a linear combination of area normalized detection patterns p_j^k :

$$I_j(t) = \sum_{k=1}^{n} w^k(t)\, p_j^k \quad (9)$$

where k stands for a particular emitter with a specific detection pattern, n is the number of different emitters with different detection patterns and $w^k(t)$ is the contribution of the k^{th} fluorescent species to the total fluorescence signal at time t.

Equation. (1) is an over-determined set of linear equations, provided the number of detection channels is higher than the number of different emitters. Assuming that the photon detection obeys a Poissonian distribution and applying singular value decomposition, the solution of the Eq. (1) can be written as follows:

$$w^k(t) = \sum_{j=1}^{N} f_j^k I_j(t) \tag{10}$$

where N is the number of detection channels and f_j^k is a discrete filter function, which is constructed from the area normalized detection patterns of the different fluorescence species and the total intensities of the compound signal in detection channels. Explicitly, f_j^k is given by:

$$f_j^k = \left(\left[\hat{M}^T \cdot diag \left\langle I_j(t) \right\rangle_t^{-1} \cdot \hat{M} \right]^{-1} \cdot \hat{M}^T \cdot diag \left\langle I_j(t) \right\rangle_t^{-1} \right)_{kj} \tag{11}$$

where the matrix elements are:

$$\hat{M}_{jk} = p_j^k \tag{12}$$

Finally, the intensity normalized correlation function of the k^{th} species with l^{th} species (for auto-correlation $k = l$, for cross-correlation $k \neq l$) is calculated as:

$$G^{kl}(\tau) = \frac{\left\langle w^k(t) w^l(t+\tau) \right\rangle_t}{\left\langle w^k(t) \right\rangle_t \left\langle w^l(t) \right\rangle_t} = \frac{\sum_{i=1}^{N} \sum_{j=1}^{N} f_i^k f_j^l \left\langle I_i(t) I_j(t+\tau) \right\rangle_t}{\sum_{i=1}^{N} \sum_{j=1}^{N} f_i^k f_j^l \left\langle I_i(t) \right\rangle_t \left\langle I_j(t) \right\rangle_t} \tag{13}$$

In the case of pulsed excitation and pulsed STED detection (Figure 2) the first pattern p_1 corresponding to super-resolved emission is obtained from the experimental excited state decay without any STED applied. The decay pattern p_2 for the ring emission is then obtained by subtracting a scaled super-resolution pattern $a^* p_1$ from the overall average experimental decay $<I(t)>$. The scaling factor a is obtained by fitting the tail of the overall average experimental decay $<I(t)>$ with the super-resolved pattern p_1. This procedure is based on the fact that after the STED pulse is over, the measured fluorescence decay returns to its intrinsic kinetics. Here, tail-fitting was usually performed for decay between 3 ns – 12.5 ns.
For the case of pulsed excitation and cw STED depletion the overall average experimental decay $<I(t)>$ was fitted by a sum of three exponentials. The value of the longest lifetime influences the resulting spatial resolution and can be fixed during the excited state decay fitting. Reconstructed decay for every lifetime component corresponds to one pattern p_i. For simulations the instrument response function (IRF) was a delta function.
The correlation function with the best spatial resolution is obtained as an autocorrelation function of the super-resolved pattern for the pulsed depletion or of the pattern with the longest lifetime for cw depletion.

ADDITIONAL MATERIALS AND METHODS

Line-scan gated STED with pulsed excitation and cw depletion

Line-scan FCS data analysis is not limited to pulsed excitation and pulsed depletion, and to TTTR data acquisition format. A proof-of-principle experiment measuring diffusion coefficients of DOPE-Atto488 in SLBs on glass (DOPC:DOPS 4:1, lipid to dye ratio 1:50 000) at and below diffraction limited resolution was performed using a commercial setup for gated-STED (SP5, Leica, Germany) in the test facility at Leica Microsystems in Mannheim. The commercial gated-STED microscope uses pulsed excitation together with cw depletion and gated detection to improve the spatial resolution (9).

The acquisition settings were: excitation by 30% intensity of 494 nm spectral band of white-light laser at 80 MHz, depletion by 100 mW cw laser at 592 nm (STED only), HyD detector operated at 750V with a 1-6.5 ns gate, detection bandpass 500-585 nm, notch filter for 488 and 592 nm, xt scan frequency 8000 Hz (resonant scanner), bidirectional scan, 512 pixels per line, 29.7 nm per pixel (15.2 µm total length, zoom 10.2), 100x 1.4 NA oil STED objective. The measurement time was 60 s and data were exported as 117 pc of xt scan (512x8192) TIFF files each.
The TIFF files for each measurement were converted into a single TTTR like file. Single photon events were created from pixels containing non-zero values. Each photon event was assigned a position along the scanned line (x coordinate) and time after the start of the excitation (t coordinate). The shift between forward and backward lines was optimized by maximizing the correlation between consecutive lines. The resulting data file containing the single photon events based file was then used for our fast multiple-tau direct correlation algorithm, providing the same output as TTTR data.
The obtained spatio-temporal correlation functions (Fig. S3) could be fitted with a single component model and returned expected values for both spot radii (186 nm for confocal and 57 nm for gSTED) and diffusion coefficients (3.85 $\mu m^2 s^{-1}$ and 3.25 $\mu m^2 s^{-1}$). This shows that line-scan FCS data acquisition and analysis can be successfully used with various hardware and data formats. Moreover, line-scan FCS combined with SLBs on glass is a good tool to test the spatial resolution of fluorescence microscopes as single dye molecules are the best approximation of a point source and it is not necessary to correct the obtained resolution values as is the case with fluorescent beads. The main limitation remains the line frequency of the scanner, which must be faster than the average resident time of molecules within the detection spot.

Monte-Carlo simulation of line-scan STED-FCS experiments

To test the performance of the correlation algorithm and to compare the gating and filtering data analysis options for cw STED with gated excitation (gSTED), Monte-Carlo simulations of line scan experiments were performed. Our simulations extend the work of Wohland et al. (10) by adding a resonant line scan and excited state lifetime features. Particles with a fluorescent lifetime of 4 ns and a diffusion coefficient of 2 $\mu m^2 s^{-1}$ were simulated to be subject to 2D Brownian diffusion in a 8 µm x 4 µm rectangle simulation box with periodic boundaries. A fraction of the molecules was allowed to be immobilized and/or to become subject to photobleaching. The simulations were run at 10 MHz clock for 60 s. The Gaussian excitation spot of radius 300 nm was overlaid by a STED donut, which was approximated by a parabolic function, and both are simultaneously scanned along a 4 µm long line with a frequency of 8 kHz. The detection efficiency was assumed to be uniform and the molecular brightness in the centre of the excitation spot with no STED was 100 kHz per molecule. STED represented an additional de-excitation pathway from the excited state of the molecule, the rate of which was position dependent. At each point the decay of the molecule's excited state was assumed to be monoexponential with a rate constant being the sum of the intrinsic fluorescence rate and STED depletion rate. The brightness of the molecule was adjusted accordingly, assuming a fluorescence quantum yield without STED equal to one.

Area integrated correlation function

In molecular diffusion, when the only process taking place is the movement of molecules within the plane, molecules cannot disappear from the image of that plane. This means that the probability of detecting its signal within that plane is constant over time. The spatial-temporal correlation function expresses the probability that a photon from the same molecule at given position and at certain time later is detected. Therefore, for planar diffusion, the sum of correlation values *G(t,x,y)* for all points within the *xy* plane is constant for any correlation time *t*.

$$\iint_{-\infty}^{+\infty} G(t,x,y)dxdy = const \quad (14)$$

The spatial-temporal correlation function for the entire plane (xy) can be obtained through image correlation. As image acquisition is not sufficiently fast, we used line correlation *G(t,r)* where *r* is the distance between the points, which is faster than image correlation and still spatially resolved. If the molecular mobility is isotropic (no direction preferred when averaged over the image and time), a rotational symmetry for the area correlation function can be assumed. Thus the integral of area correlation function can be obtained by integrating the line correlation function along the full angle. This results in:

$$\iint_{-\infty}^{+\infty} G(t,x,y)dxdy = \int_{0}^{+\infty} 2\pi r G(t,r)dr = const \quad (15)$$

The simplest spatio-temporal model of free 2D-diffusion with Gaussian detection areas results in

$$G(t,r) = \frac{A}{4Dt+{w_0}^2} e^{-\frac{r^2}{4Dt+{w_0}^2}} \quad (16)$$

which is a constant value independent of time after integration

$$\int_{0}^{+\infty} 2\pi r \frac{A}{4Dt+{w_0}^2} e^{-\frac{r^2}{4Dt+{w_0}^2}} dx = \left[\pi A e^{-\frac{x^2}{4Dt+{w_0}^2}} + const\right]_{0}^{+\infty} = \pi A. \quad (17)$$

For discrete, uniformly spaced line correlation function of experimental data, the equation to use for calculating the area integrated correlation function $G_A(t)$ for each correlation time t_j is

$$G_A(t_j) = \sum_{i=-n}^{n} x_i G(t_j, x_i) \quad (18)$$

where n is the number of distances for which the temporal correlation is calculated in both directions, resulting in total 2n+1 temporal correlations. The limitation is the finite distance for which the correlations are calculated. This affects mainly the long correlation times at which there is a significant probability that the molecule diffuses out of the maximum correlation distance.

SUPPORTING REFERENCES

1. Ries, J., S. Chiantia, and P. Schwille. 2009. Accurate determination of membrane dynamics with line-scan FCS. Biophys J 96:1999-2008.
2. Digman, M. A., C. M. Brown, A. R. Horwitz, P. Sengupta, W. W. Mantulin, and E. Gratton. 2005. Spatio-temporal fluorescence fluctuation analysis of paxillin-EGFP in cellular adhesions using scanning FCS, ICS and PCH. Biophys J 88:372a-372a.

3. Gregor, I., and J. Enderlein. 2007. Time-resolved methods in biophysics. 3. Fluorescence lifetime correlation spectroscopy. Photoch Photobio Sci 6:13-18.
4. Benda, A., V. Fagul'ová, A. Deyneka, J. Enderlein, and M. Hof. 2006. Fluorescence lifetime correlation spectroscopy combined with lifetime tuning: New perspectives in supported phospholipid bilayer research. Langmuir 22:9580-9585.
5. Böhmer, M., M. Wahl, H. J. Rahn, R. Erdmann, and J. Enderlein. 2002. Time-resolved fluorescence correlation spectroscopy. Chem Phys Lett 353:439-445.
6. Benda, A., P. Kapusta, M. Hof, and K. Gaus. 2014. Fluorescence spectral correlation spectroscopy (FSCS) for probes with highly overlapping emission spectra. Opt Express 22:2973-2988.
7. Felekyan, S., S. Kalinin, A. Valeri, and C. A. M. Seidel. 2009. Filtered FCS and Species Cross Correlation Function. Proc Spie 7183.
8. Štefl, M., A. Benda, I. Gregor, and M. Hof. 2014. The fast polarization modulation based dual-focus fluorescence correlation spectroscopy. Opt Express 22:885-899.
9. Vicidomini, G., A. Schönle, H. Ta, K. Y. Han, G. Moneron, C. Eggeling, and S. W. Hell. 2013. STED nanoscopy with time-gated detection: theoretical and experimental aspects. PloS one 8:e54421.
10. Wohland, T., R. Rigler, and H. Vogel. 2001. The standard deviation in fluorescence correlation spectroscopy. Biophys J 80:2987-2999.
11. Dertinger, T., I. Gregor, I. von der Hocht, R. Erdmann, B. Krämer, F. Koberling, R. Hartmann, and J. Enderlein. 2006. Measuring precise diffusion coefficients with two-focus fluorescence correlation spectroscopy. P Soc Photo-Opt Ins 6092.

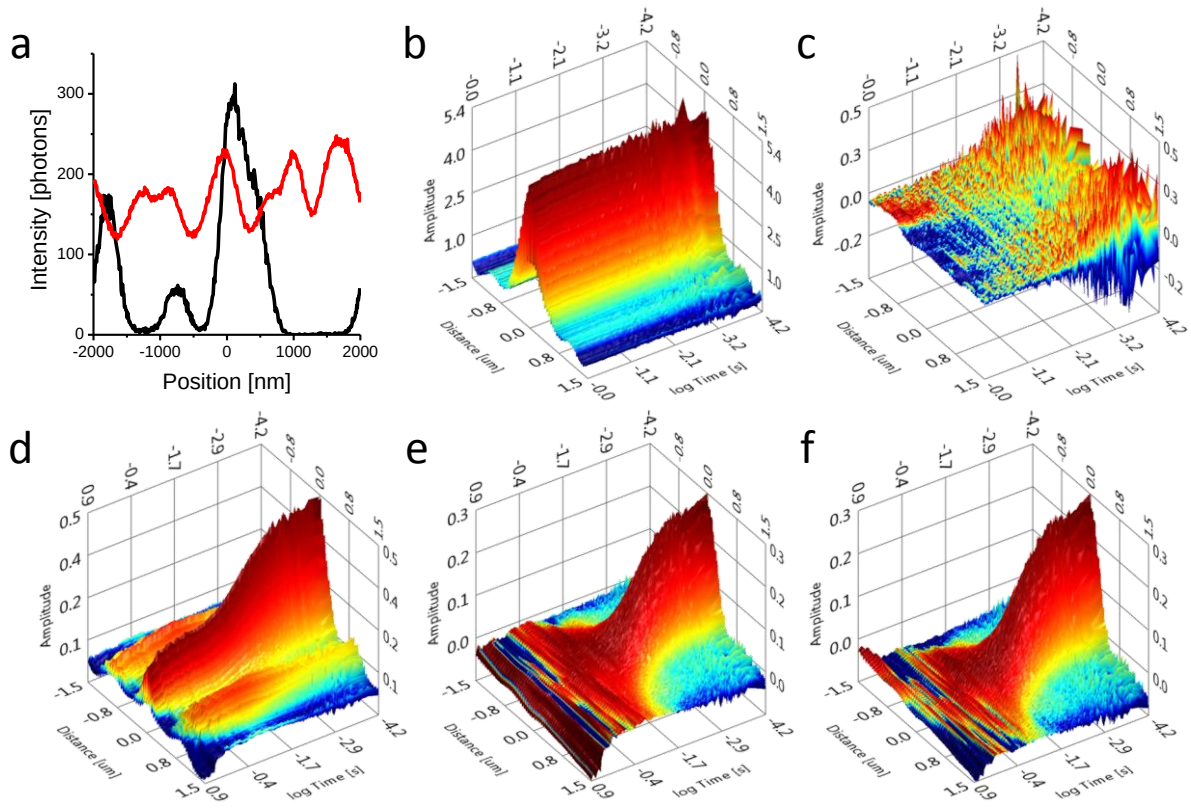

Figure S1 Correction of spatio-temporal correlation functions for heterogeneous immobile fraction and homogenous photobleaching.

(**a**) Intensity profiles along the scanned line for Monte-Carlo simulated data of immobile particles (black line) and a mixture of immobile particles with freely diffusing particles (red line). (**b-c**) The spatio-temporal correlation function of fixed particles without spatial profile correction (b) has a strong time-constant spatial correlation. After the spatial profile correction (c) no spatial correlation is left. (**d-f**) Uncorrected spatio-temporal correlation function (d) for a mixture of freely diffusing particles with slowly photobleached immobile background. The spatial profile correction removes the time constant spatial correlations (e) and subsequent photobleaching correction (f) recovers correlation function for mobile particles only.

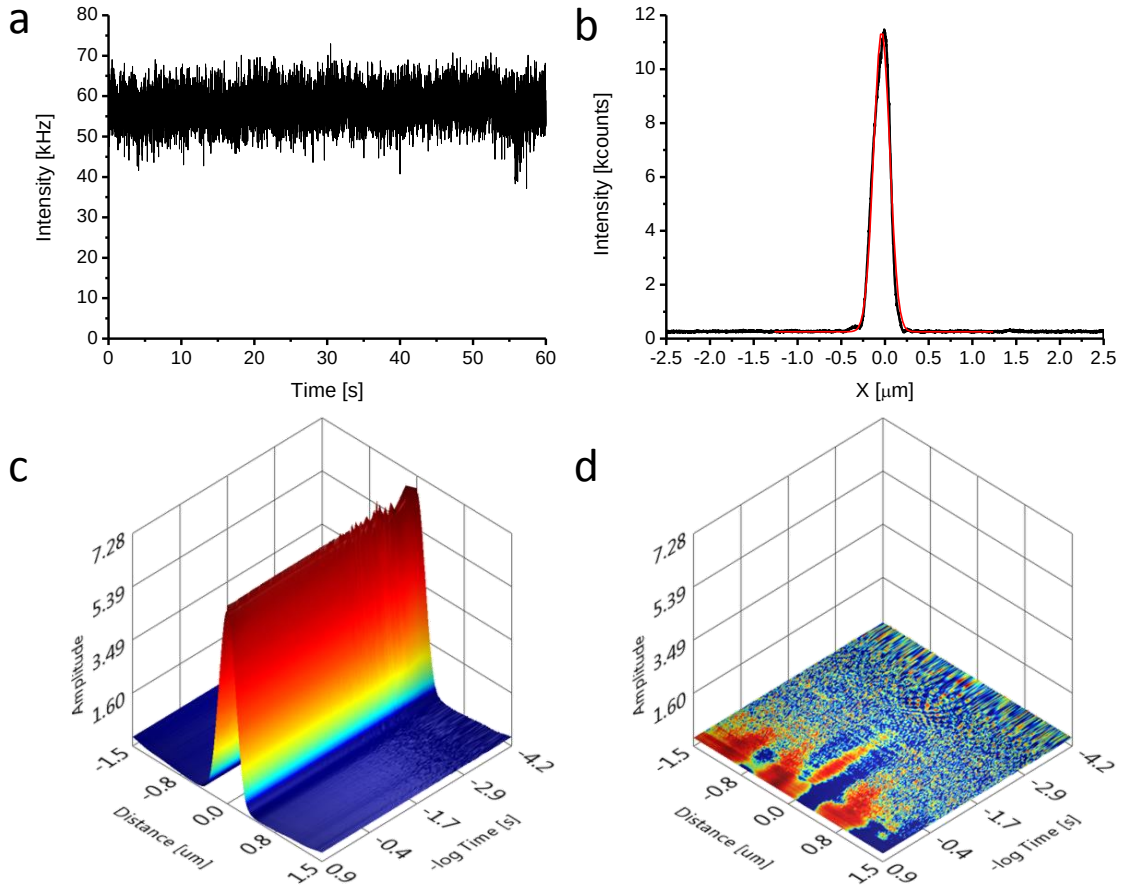

Figure S2 Experimental test of scanner and sample stability.
An immobile gold bead was scanned for 60 s using the standard scan settings (bidirectional resonant line scan, 7920 Hz, 100x oil immersion objective NA1.4, zoom 30x). An excitation light of 640 nm laser was scattered by the bead and after attenuation detected by SPAD detector. (**a-b**) The intensity time trace with 6.3 ms sampling shows no significant trend or oscillations. The spatial profile of the bead along the scanned x-axis (b, black line) is fitted by a Gauss function (b, red line), giving a radius of 185 nm. (**c**) The uncorrected spatio-temporal correlation function has a strong time-constant spatial correlation. (**d**) After the spatial profile correction, no significant correlation can be observed up to 100 ms timescale and only negligible correlations at longer time scales.

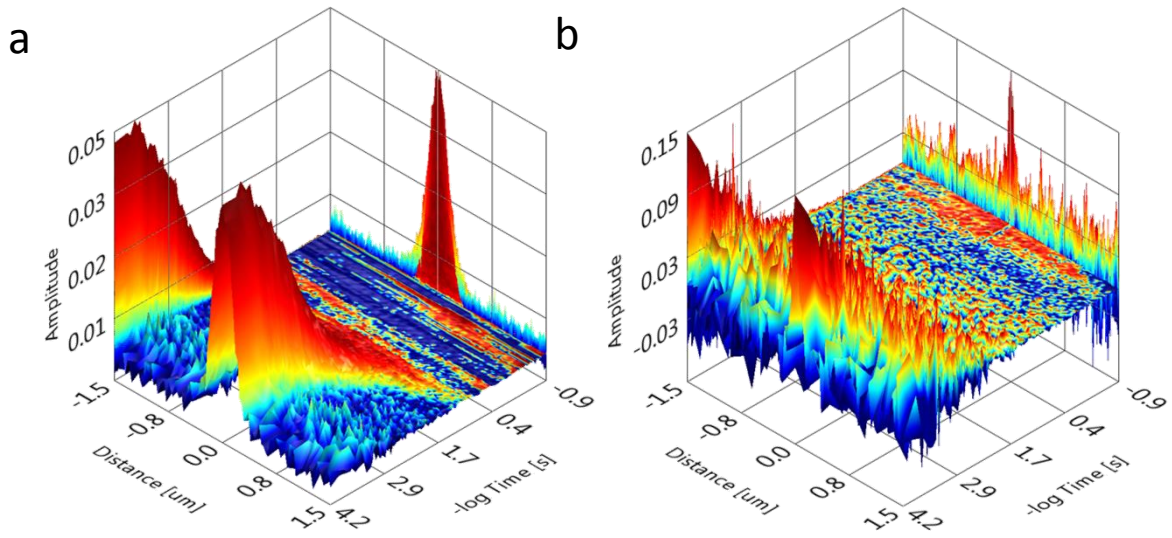

Figure S3 Line-scan gSTED-FCS with TIFF data format.
(**a-b**) Spatio-temporal correlation functions of DOPE-Atto488 in SLBs (DOPC:DOPS 4:1, dye to lipid ratio 1:50 000) on glass measured under confocal (a) and gated-STED conditions (b). The spot radii from the fits are 186 nm and 57 nm for confocal and gated-STED, respectively, and the diffusion coefficients are 3.85 $\mu m^2 s^{-1}$ and 3.25 $\mu m^2 s^{-1}$, respectively.

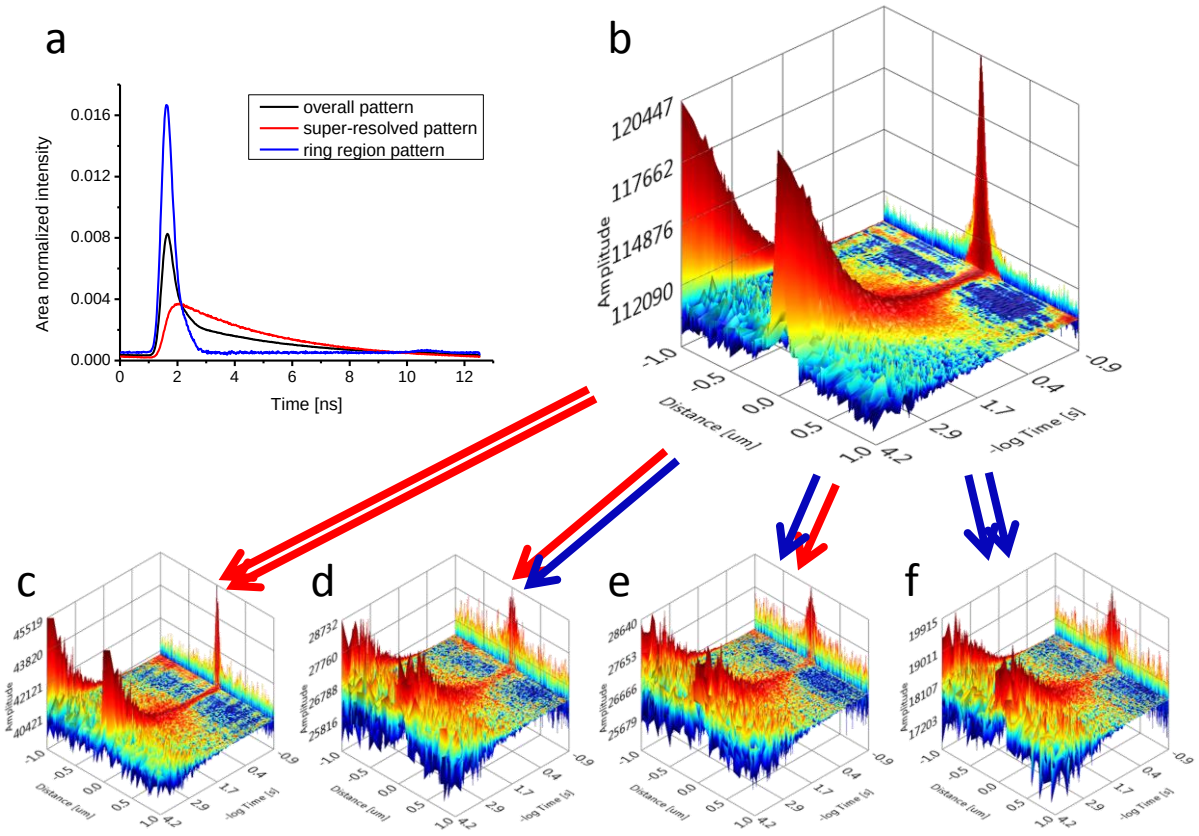

Figure S4 Splitting of the overall spatio-temporal correlation function by filtered FCS. (**a**) The experimentally obtained TCSPC pattern (black line) for DOPE-Atto647N in SLBs made of DOPC on glass (lipid to dye ratio 1:50 000, 640 nm excitation at 10 µW, 750 nm depletion at 100 mW, detection 660-700 m, measurement time 5 min) is a linear combination of TCSPC patterns for fluorescence of non-depleted molecules located in the donut zero region (red line) and a fast decaying component (blue line) originating from fluorescence before depletion in the ring region. (**b**) The overall spatio-temporal correlation function from raw data without filtering. (**c**) The filtered spatio-temporal auto-correlation function for central region fluorescence. (**d**) The filtered spatio-temporal cross-correlation function of the central region and ring fluorescence. (**e**) The filtered spatio-temporal cross-correlation function of the ring and central region fluorescence. (**f**) The filtered spatio-temporal auto-correlation function for ring fluorescence. The presented correlation functions are not intensity normalized. The overall correlation function (b) is a sum of the four filtered correlation functions (c-f). The PSF width for filtered correlation functions is 40 nm (c), 100 nm (d), 95 nm (e) and 130 nm (f).

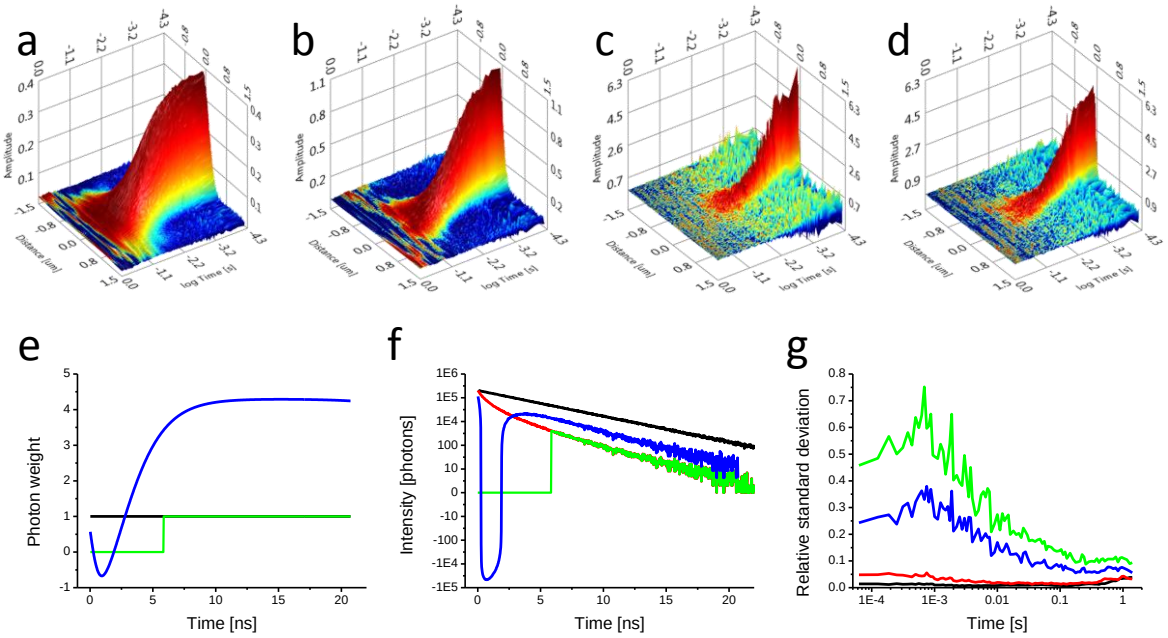

Figure S5 Monte-Carlo simulation of line-scan, filtered cw STED-FCS.
(**a-d**) Spatio-temporal correlation functions for confocal (a), cw STED (b), gated cw STED (c) and filtered cw STED (d) show decreasing PSF width from 300 nm for confocal, 175 nm for cw STED down to 75 nm for gated and filtered cw STED. The fitted diffusion coefficient is 2 $\mu m^2 s^{-1}$ for all cases. (**e**) Filters for photon weighting based on the photon arrival time after excitation. Confocal and cw STED uses all photons equally (black line), gated cw discards photons arriving before 6 ns (green line) and filtered cw STED weights photon by a filter calculated for the longest decay component (blue line). (**f**) TCSPC histograms show that the confocal signal is mono-exponential (black line) whereas the cw STED signal is multi-exponential (red line) due to the cw depletion. The gated cw STED histogram contains only the late arriving photons (green line) and filtered cw STED histogram (blue line) enhances late photons but uses the whole data range. (**g**) Both gating and filtering can achieve identical resolution (75 nm in this case, no background included in simulations), but filtering (blue line) is more efficient in relation to signal usage and the obtained correlations have almost two times lower relative standard deviation than gating (green line).

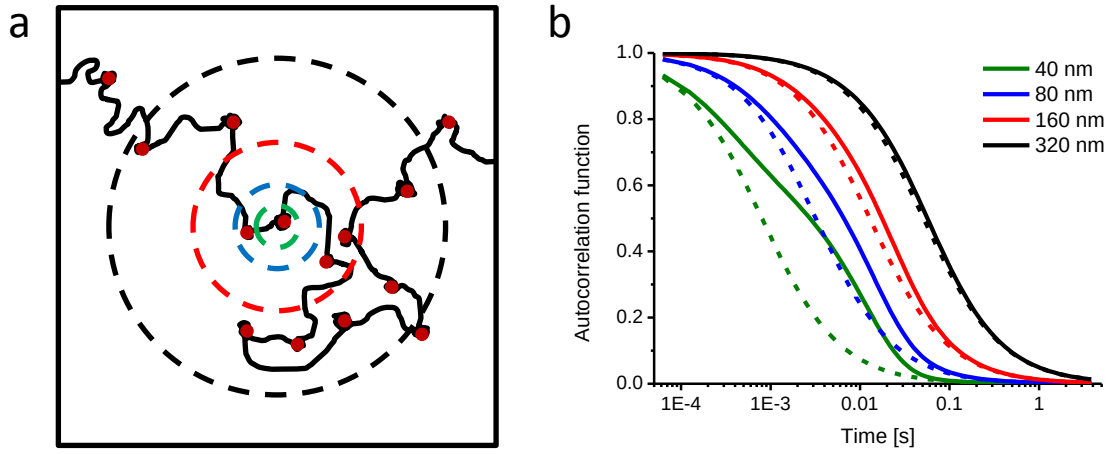

Figure S6 Principle of variable spot STED-FCS with transient binding.
(**a**) Schematic of particle diffusion with transient trapping (red dots) in detection spots of variable radius (dotted circles: 320 nm radius black, 160 nm radius red, 80 nm radius blue and 40 nm radius green). (**b**) Autocorrelation functions for laterally diffusing molecules (D = 1 $\mu m^2 s^{-1}$) that are transiently trapped at random locations (k_{on} = 100 s^{-1}, k_{off} = 100 s^{-1}) for varying detection spot radius (solid lines: 320 nm radius black, 160 nm radius red, 80 nm radius blue and 40 nm radius green). The calculation is based on the diffusion model described in Dertinger et al. (11). Autocorrelation functions for two times slower free diffusion (D = 0.5 $\mu m^2 s^{-1}$, dash lines) are shown for comparison. The time resolution of the calculations is identical to the time resolution of line scan FCS, spot size are matched to experimentally obtainable spot sizes and the diffusion coefficient is set to a typical value observed for labelled lipids in the plasma membrane.

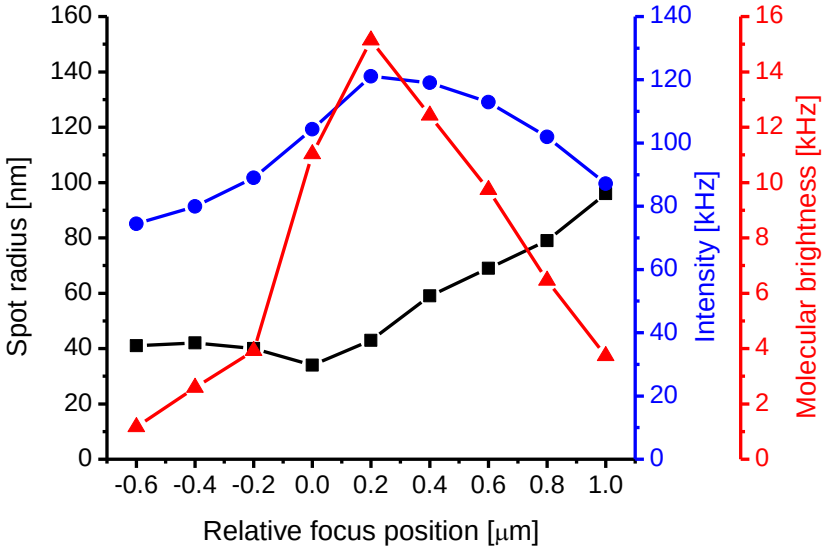

Figure S7 Axial dependence of STED-FCS measurements.
SLBs made of DOPC on glass and labelled with DOPE-Atto647N in lipid to dye ratio 1:100 000 were measured by line-scan STED-FCS (640 nm excitation at 10 µW, 750 nm depletion at 100 mW, detection 660-700 m, filtered correlation) at different focus positions (axial direction) relative to the sample. Axial dependence of spot radius (black squares), overall fluorescence intensity (blue circles) and the apparent molecular brightness (red triangles) on the focus position relative to the sample position are shown. Data indicate that the position of the best spatial resolution does not have to coincide with the position of the highest detected overall intensity. A small misalignment along the z-axis (400 nm) can cause a significant difference in actual spot radius (from 40 nm to 60 nm).

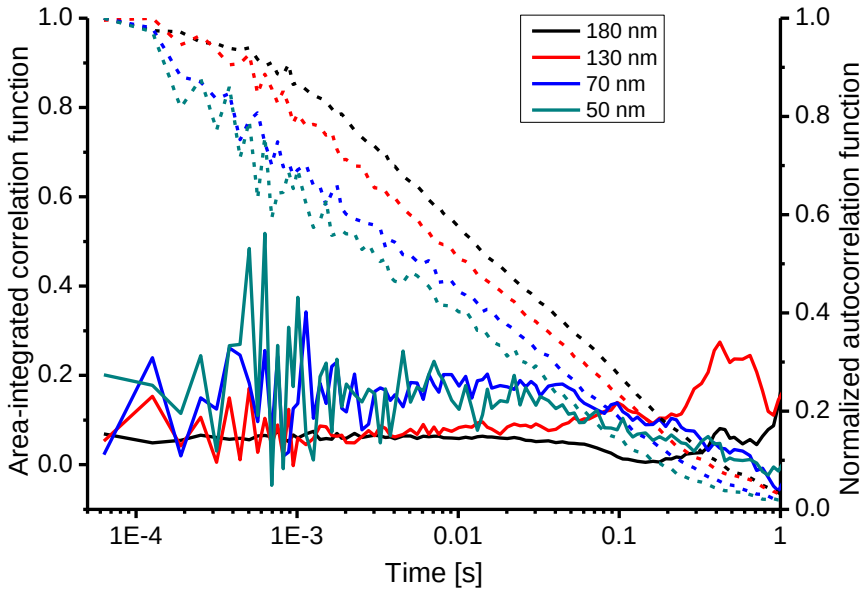

Figure S8 Area-integrated correlation function.
Area-integrated correlation functions (solid lines) and temporal autocorrelation functions (dashed lines) for DOPE-Atto647N in supported lipid bilayers on glass (DOPC:DOPS 4:1, lipid to dye ratio 20 000:1, 640 nm excitation at 10 µW) at increasing STED powers, decreasing the spot radius from 180 nm (black line) to 130 nm (red line), 70 nm (blue line) and 50 nm (dark green line). The constant values of area-integrated correlation functions at short times for each spot size are indicative that the fast decays of the temporal autocorrelation functions are not related to dye photo-physics induced by the intensive STED laser but indeed caused by 2D diffusion.

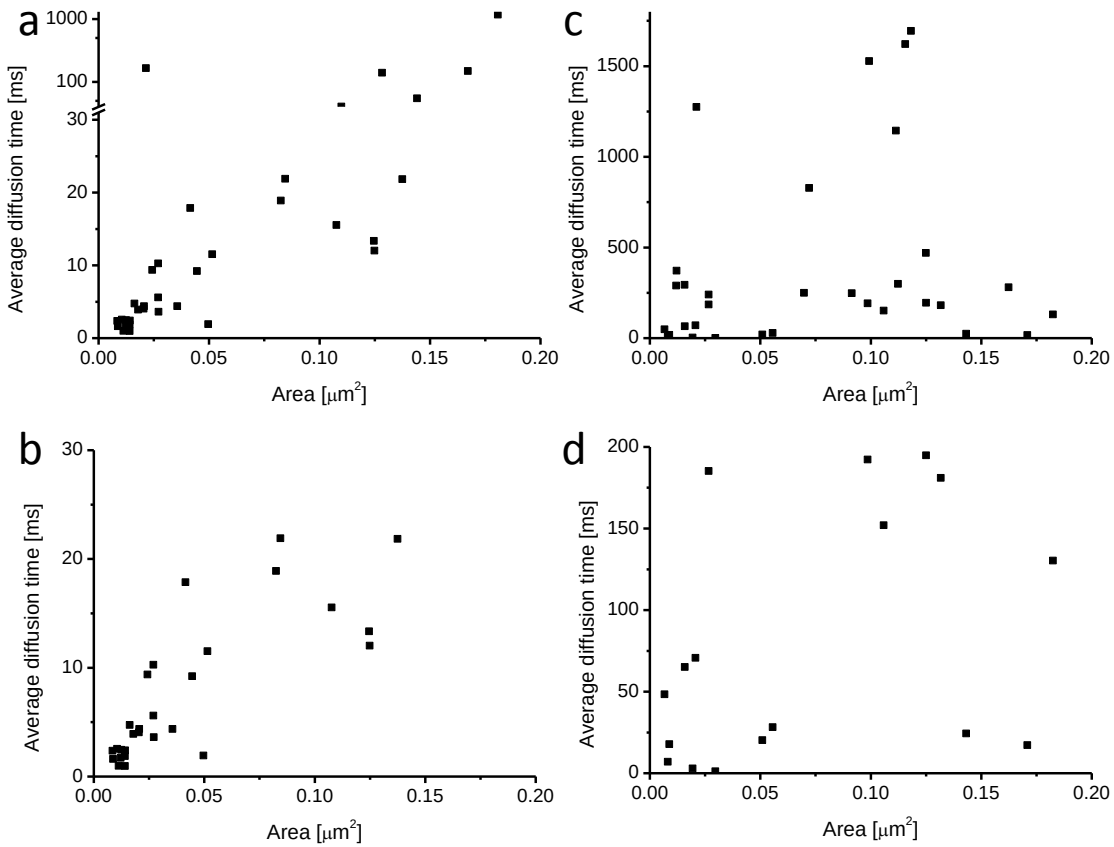

Figure S9 Variable spot STED-FCS in cells.
The average diffusion time is plotted against the spot area for DOPE-Atto647N (**a-b**) and Atto647N-SM (**c-d**) in COS7 cells. Each data point represents one measurement. The lower graphs (b, d) are zooms of graphs (a, c). The raw data are identical to the raw data used in Figure 5a and 5b. The average diffusion time was obtained as the time at which the correlation function at zero spatial difference declines to a half of its value at zero lag time. The spot area was obtained from the spot radius at zero lag time using a Gaussian approximation.

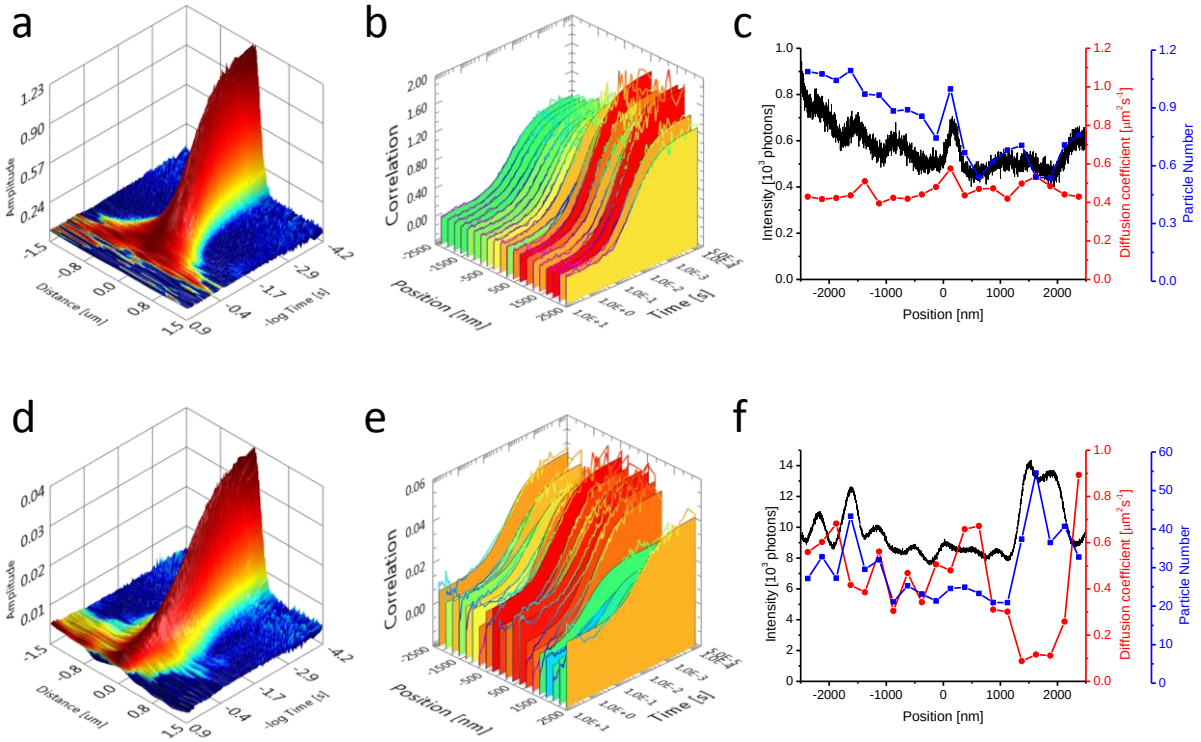

Figure S10 Comparison of DOPE-Atto647N with DOPE-Oregon Green 488. Confocal line scan FCS was performed on the plasma membrane of HeLa cells. The cells were labelled either with DOPE-Oregon Green 488 (**a-c**) or with DOPE-Atto647N (**d-f**). For DOPE-Oregon Green 488 acquisitions, the 488 nm line of cw Argon laser at 5 µW, emission bandpass filter HQ525/50 and 7.92 kHz bidirectional resonant scanner were used. For DOPE-Atto647N acquisitions, a 640 nm pulsed laser at 5 µW, emission bandpass filter HQ680/40 and 7.92 kHz bidirectional resonant scanner were used. The spatio-temporal correlation function for DOPE-Oregon Green 488 (**a**) could be fitted to a one-component model (D = 0.44 $\mu m^2 s^{-1}$, w_0 = 172 nm), the spatio-temporal correlation function for DOPE-Atto647N (**d**) needed a two-component model (D_{fast} = 0.727 $\mu m^2 s^{-1}$, D_{slow} = 0.013 $\mu m^2 s^{-1}$, w_0 = 197 nm). Temporal autocorrelation functions (**b, e**) at different points along the scanned line were fit using a single component model. (**c, f**) The diffusion coefficients and particle numbers (obtained from the one-component fit, b and e) are plotted together with the overall fluorescence intensity as a function of the position along the line. The average diffusion coefficient for DOPE-Oregon Green 488 was 0.457 ± 0.05 $\mu m^2 s^{-1}$; the average diffusion coefficient for DOPE-Atto647N was 0.436 ± 0.21 $\mu m^2 s^{-1}$.